Available online at www.sciencedirect.com

SciVerse ScienceDirect

Ceramics International 38 (2012) 4997–5006

CERAMICS INTERNATIONAL

www.elsevier.com/locate/ceramint

Comparison of solid state and sol–gel derived calcium aluminate coated graphite and characterization of prepared refractory composite

S. Mukhopadhyay *, S. Dutta

Ceramic Engg. Division, Department of Chemical Technology, University of Calcutta, 92 APC Road, Kolkata 700009, India

Received 19 January 2012; received in revised form 29 February 2012; accepted 29 February 2012
Available online 7 March 2012

Abstract

This paper entails an extended investigation on sol–gel thin film of calcium aluminate ($CaAl_2O_4$) over graphite flakes that improved their oxidation resistance and water wettability. The commercial preparation of calcium aluminate has been compared with the sol–gel synthesis by differential thermal analysis (DTA) and X-ray diffraction (XRD) to assess the feasibility of the latter for coating preparation. Poorly crystalline nanostructured Ca-doped γ-Al_2O_3 is considered to be an important intermediate for this preparation. Scanning electron microscopy (SEM) and energy dispersive spectroscopy (EDS) of the calcined gel have been carried out to ascertain its composition. Quantitative chemical analysis of sol gel derived calcium aluminate was also estimated. Atomic force microscopy (AFM) has been conducted to ensure the evolution of hydrophilic nanosized cementitious phases on graphite. Zeta potential values of coated and uncoated graphites with increasing pH have also been determined to distinguish between their compatibility in a refractory castable matrix. Improved physical properties of that high alumina castable containing coated graphite, e.g. apparent porosity (AP), bulk density (BD), cold crushing strength (CCS) have been measured to evaluate the refractory quality. The reasons for its better performance are explored by taking further insight on the microstructural analyses of the fired castable (1500 °C) soaked for an extended period.

Keywords: A. Sol–gel processes; B. Electron microscopy; D. Graphite; $CaAl_2O_4$; E. Refractory castables

1. Introduction

Several attempts are going on to develop carbon containing monolithic castables and ensure their successful performance in steel plants [1–3] .The most important factor during preparation of this refractory is to make the carbon wettable with minimum water that could disperse and result in a dense structure in due course. The second important factor is to hold that carbon in that structure for a longer period. In the carbon–oxygen system, many condensed phases and gas species are generated, namely C(s), CO_2(s,l), O_2(l,g), CO(g), CO_2(g), etc. [4]. As such the oxidizing atmosphere of furnaces leads to substantial loss of carbon present in the refractories. It is possible to incorporate carbon in different refractory linings in the form of coke, carbon black and graphite. Among these solids, flaky graphite has been chosen in our previous work [5–8], due to its crystalline nature, superior bulk density, overall stability and other advantages. Viscosity of liquid binders and impregnating agents (e.g. resin, tar, pitch) should be carefully monitored for installation of castables; nevertheless, these have been utilized in refractories as carbonaceous materials since decades [9,10]. These two are excluded from our investigation to avoid the liberation of hazardous pyrolysis products. Many fruitful efforts have already been reported for improving the water wettability and thermal stability of graphite [11–13]. We adopted a modified sol gel route for surface treatment of graphite by spinel and mullite thin films [5–8]. It assured stabilization of graphite and substantially overcame the two impediments mentioned above. The chemical treatment of graphite with sol–gel derived calcium aluminate, in this regard, has been studied in our recent communication [14]. It is well documented that the wet chemical synthesis of calcium aluminate results in high surface area, controlled chemical composition, homogeneous distribution of the constituents and relatively low temperature requirement [15–19]. The use of calcium aluminate cement in refractory applications still dominates its other applications and

* Corresponding author. Tel.: +91 33 2350 8386; fax: +91 33 23519755.
E-mail address: msunanda_cct@yahoo.co.in (S. Mukhopadhyay).

0272-8842/$36.00
doi:10.1016/j.ceramint.2012.02.096

it is compatible to both high alumina and basic castables. The other reasons for developing calcium aluminate coated graphite have been explained in that previous communication with a brief description of its synthesis and characterization. This paper includes further insight on that work and an extended investigation on the characteristics and performance of a high alumina castable containing that coated graphite. In this regard a comparison between the traditional solid state preparation and sol–gel processing of calcium aluminate has also been highlighted to emphasize here the relevance of the latter.

2. Experimental

Synthesis of calcium aluminate precursor by sol–gel route has been discussed in our earlier work along with the preparation of coated graphite by that precursor [14]. The sol–gel process employed here is quite easy-to-use involving a hybrid set of precursors e.g. aluminium-sec-butoxide and hydrated calcium nitrate. Propanol, acetylacetone, deionised water, acetic and nitric acids were the other important chemicals for sol preparation involving less expensive equipments. Supplied graphite (97% carbon) was slowly mixed to the binary sol, dried, sieved and calcined (600 °C) to prepare calcium aluminate coated graphite for incorporation in a monolithic refractory composite. A parallel attempt has been done here to derive calcium aluminate as followed conventionally in cement industries. However unlike bauxite and limestone, we used purer and finer grades of these materials. For this purpose, LR grade calcium carbonate powder (assay >98.5%, Merck) and reactive alumina ($Al_2O_3 > 99.5\%$, specific surface area 4.6 m^2/g, INDAL) were thoroughly mixed in a slurry form, dried and milled again, keeping the mole ratio of (1:1) to maintain ($CaO:Al_2O_3$) stoichiometry. The DTA and XRD of this mix were compared with that obtained for sol–gel derived calcium aluminate powder. XRD patterns of the main precursor gel, namely boehmite (γ-AlOOH) calcined at 300 and 500 °C, had also been studied to understand the evolution of nano crystalline γ-Al_2O_3 as performed earlier in a similar work [20]. The XRD phase evolution of dried and heat-treated calcium aluminate gels were also investigated within a broad temperature spectrum, namely, 110, 600, 750, 930, 1100 and 1400 °C. The SEM (with EDS) of this gel calcined at 930 °C and 1400 °C were also carried out to confirm the composition of the cementitious phases in those micrographs. The quantitative chemical analysis of sol–gel calcium aluminate powder (1400 °C) was estimated to substantiate the EDS results. AFM of coated graphite was analysed to verify the existence of hydrophilic nanodimensional calcium aluminate enriched phases over graphite flakes.

As these coated graphites have been incorporated to refractory castable slurry [14], the comparison of changes in zeta potentials between coated and uncoated graphites was also studied with respect to the variation of pH. The monolithic castable composite containing graphite (5.0%) was a low cement (4.0%) formulation with white fused alumina aggregates (72%). The matrix part (28%) contained microsilica, spinel ($MgAl_2O_4$), reactive alumina, aluminium powder, sodium hexa-metaphosphate including the cement fines with graphite. Its fabrication and heat treatment (110 °C, 900 °C and 1500 °C) had been outlined in our previous articles [5–8]. C^+ and C^- codes were used respectively for castables containing coated and uncoated graphites. Determination of AP, CCS, BD values of heat treated castables has been conducted in accordance with ASTM C133-94, C133-97 and C20-00 specifications. Micrographs of C^+ castables fired at 1500 °C (with 5 h soaking) were thoroughly examined finally with respective EDS reports at several points to explain its better performance.

Chemical analysis of cement composition was done quantitatively by rapid estimation (by oxalic–tartaric–citric acid mixture) together with the conventional EDTA method, taking cement solution in concentrated HCl [21]. Zeta potential vs. pH plots were taken by the Malvern Zetasizer Nanoseries instrument (Model ZEN 2600) using deionised water, HCl and NH_4OH in proper dilution (HACH SENSION model). DTA traces of both the precursors was carried out in a Shimadzu instrument (DT-40 model) in air at a rate of 10 °C/min. XRD patterns were obtained from 'Philips Analytical Instrument', PANalytical (XPERT-PRO) model with Ni-filtered CuKα radiation. SEM/EDS experiment was conducted with Hitachi S-3400N and JEOL JSM 5200 models. For AFM analysis, the NANOSCOPE(R)IIIa (Version 5.3, 2005, Veeco instruments Limited) model was employed with a scan rate 1.2 Hz and scan range 1 mm by tapping mode operation. Differential thermogravimetry (DTG) of as-received graphite was done in NETZSCH STA 449 C (model) at a rate of 10 °C/min in air.

3. Results and discussion

Fig. 1 shows the comparison of DTA plots (up to 1000 °C) between sol–gel routed calcium aluminate gel and that of solid state precursor mix required to prepare calcium aluminate. For solid state preparation it is known that calcium carbonate decomposes at around 900 °C; however depending on the type and quantity of impurities present, surface area, morphology,

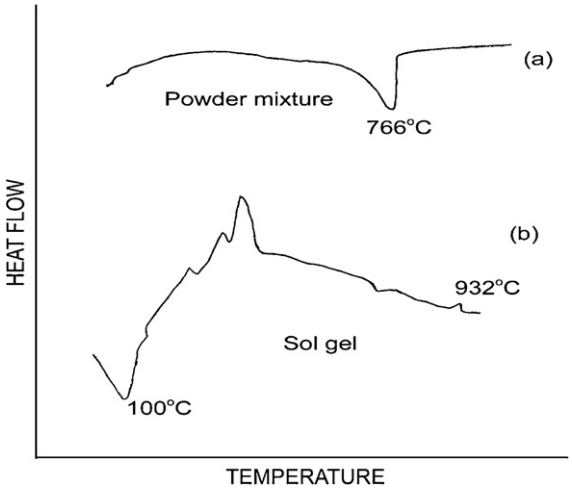

Fig. 1. DTA of (a) Al_2O_3—$CaCO_3$ powder mix and (b) sol gel derived calcium aluminate powder.

particle size distribution and partial pressure of CO_2, the dissociation temperature of limestone (calcite) can be decreased to save energy in industries [22]. In our experiment, as reactive Al_2O_3 and pure laboratory grade $CaCO_3$ fines were used, the decarboxylation temperature was further reduced to 766 °C showing no other peaks thereafter up to 1000 °C to ensure $CaAl_2O_4$ formation (Fig. 1). From literature we know the traditional preparation of calcium aluminate in cement industries requires a temperature above 1400 °C. In contrast it has been well documented that evolution of crystalline $CaAl_2O_4$ phases via sol–gel process can take place at significantly lower temperature above 900 °C [14,19]. As such graphite can be coated suitably by sol–gel $CaAl_2O_4$ before significant loss takes place by oxidation. Consequently it was difficult to conceive the preparation of coated graphite by the solid state mix of $CaCO_3$ and reactive Al_2O_3. Formation of $CaAl_2O_4$ from $CaCO_3$–Al_2O_3 mixtures has been studied between 1300 and 1500 °C by some authors [23], varying holding period between 1 and 40 h. They reported a meta-stable orthorhombic modification of calcium aluminate at 900 °C; but in our work no such result was found, may be due to the characteristics of the starting powders and the kinetics of reaction between calcite and α-Al_2O_3 [24]. We reported that sol–gel route helps to develop $CaAl_2O_4$ via the intermediate nanostructured Ca-doped γ-Al_2O_3 over flaky graphite at as low as 600 °C. It is further corroborated by Fig. 2 wherein the XRD patterns of two sets of precursors have been compared. The same oxidizing atmosphere and calcination temperature of 930 °C (2 h soaking) were retained in both cases to produce the powder phases for XRD analysis. The sol–gel process confirms the evolution of well crystallized calcium aluminate with minor amount of alumina phases. In contrast the solid state reaction yielded a mixture of Al_2O_3 (corundum) and CaO as indicated before by the DTA plot. Exposure of freshly prepared reactive CaO to the atmosphere also gave rise to some amount of $Ca(OH)_2$ in the XRD plot [22]. As such it was not feasible to prepare the coating on graphite flakes by conventional cement-forming route.

Fig. 3 shows the characteristics of the calcium aluminate gel with increasing temperature. At 110 °C (Fig. 3a), the peaks of hydrous calcium nitrate are observed that was added to the parental boehmite sol precursor for homogeneous distribution. Other less well-defined poorly crystalline regions can be due to the evolution of chelated aluminium species, as also suggested by other researchers [19]. The micrograph of precursor gel (Fig. 3a, inset) reveals the wrinkles and microbubbles present throughout the predominantly amorphous matrix due to drying and partial release of fugitives. An extended polymeric network is clear which should be helpful to build up an all pervasive thin film over graphite flakes. It has been possible due to a continuous and extensive Al–O–Al polymeric links pertaining to parental boehmite gel. Fig. 3b shows the thermal evolution of calcium aluminate at progressively higher temperatures. The small peak at 600 °C below 30° can be due to $CaCO_3$ formed (PDF: 05-0586) after atmospheric exposure of reactive CaO generated by nitrate decomposition. $CaCO_3$ formation was confirmed by the FTIR patterns of sol–gel calcium aluminate at different temperatures as elaborately discussed in our last work [14]. It also indicated presence of (AlO_6) groups and (Ca–O–Al) linkage. The other two feeble peaks for (3 1 1) and (4 0 0) planes (Fig. 3b) suggest that γ-Al_2O_3 is also present at this temperature. We therefore opine the formation of poorly crystalline nanostructured disordered Ca-doped γ-Al_2O_3 as proposed by other authors in a similar processing [25]. Calcium aluminate compounds with different ($CaO:Al_2O_3$) ratios can be crystallized with and without γ-Al_2O_3 as clarified by Douy et al. [26]. Monocalcium aluminate can be synthesised favourably via γ-Al_2O_3 formation as reported by Lavat et al. [27]. Thus at 930 °C, $CaAl_2O_4$ (orthorhombic/pseudohexagonal) can be generated in due course by heating this intermediate

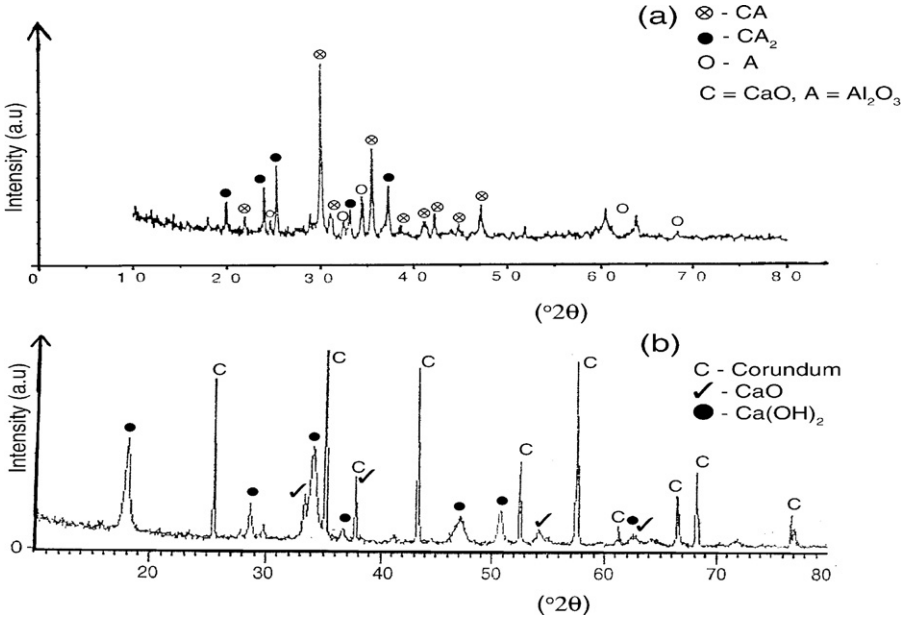

Fig. 2. XRD patterns of (a) sol gel calcium aluminate and (b) Al_2O_3—$CaCO_3$ powder mix, both calcined at 930 °C/2 h.

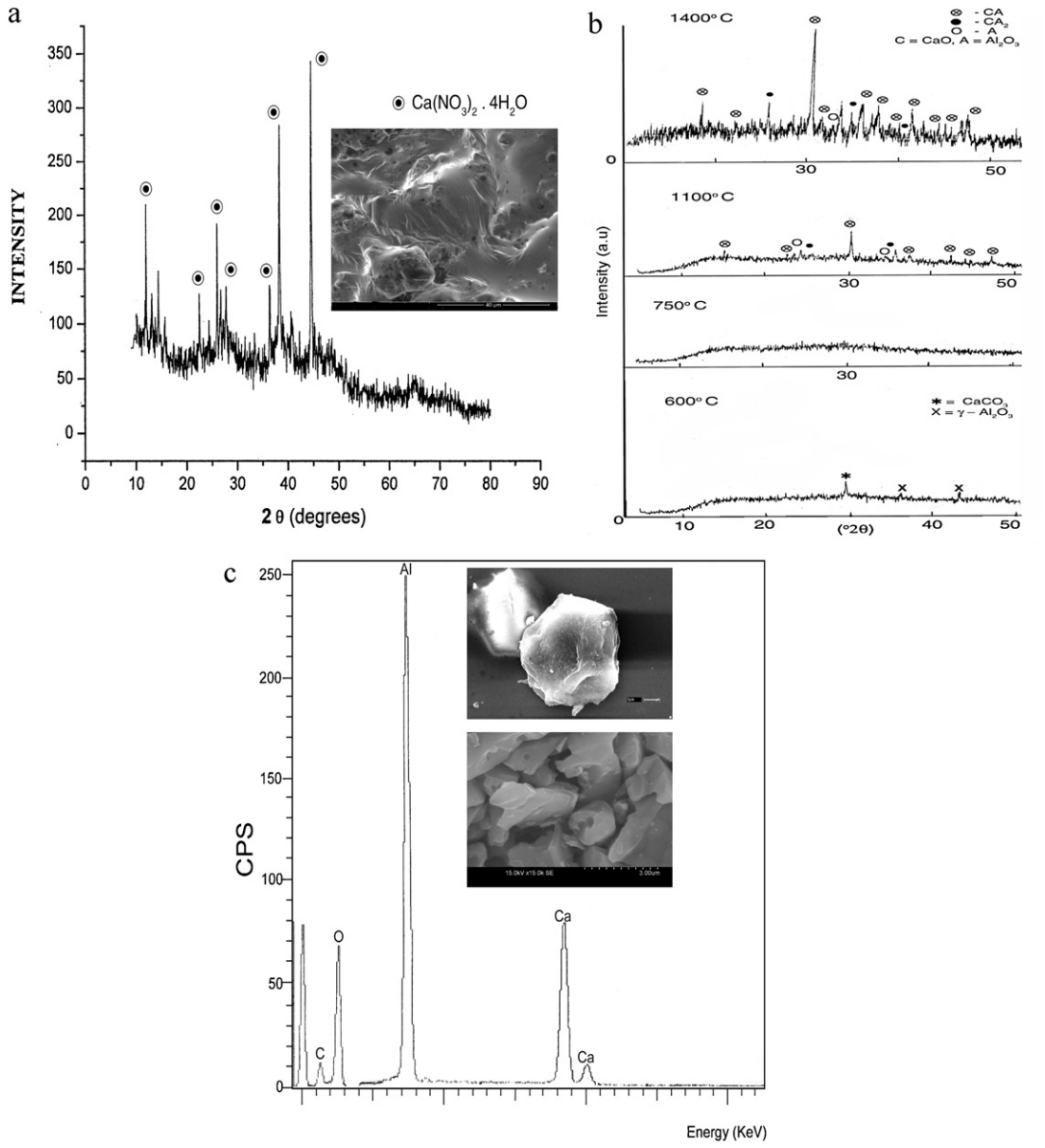

Fig. 3. (a) XRD pattern of calcium aluminate gel dried at 110 °C/2 h with the SEM of dried precursor (inset); (b) Crystalline phase evolution in calcium aluminate gel with increasing temperature (600, 750, 1100, 1400 °C) and (c) EDS and SEM (inset) of heat treated calcium aluminate gel powder: top – 930 °C, bottom – 1400 °C.

Ca-doped γ-Al_2O_3 solid solution. The broad hump at 750 °C (Fig. 3b) suggests it is predominantly amorphous, although the DTA plot shows a feeble peak at that temperature (Fig. 1). It can be ascribed to transient $C_{12}A_7$ phase [15] due to local chemical variation in the precursor composition for several reasons suggested by Kurajica et al. [19]; nonetheless $CaAl_2O_4$ is the major crystalline phase at 930 °C with higher intensity of reflections (Fig. 2a). At more elevated temperatures, i.e. 1100 °C and 1400 °C, crystallinity of monoclinic $CaAl_2O_4$ is promoted and Al_2O_3 phases become minor (Fig. 3b).

In Fig. 3c, the EDS and SEM of heat treated (930 and 1400 °C) calcium aluminate gel powders are reported. Chelated Al-alkoxide has been used to ensure controlled chemical composition of calcium aluminate phases which has been utilized later to coat graphite as a thin film. Therefore it is necessary to examine the stoichiometry of that heat treated powder, taking EDS at several points in the respective micrographs. At 930 °C, crystallization of $CaAl_2O_4$ occurs along with $CaAl_4O_7$ and minor quantity of Al_2O_3 phases (Fig. 2a). EDS plot in Fig. 3c qualitatively confirms a stoichiometry between $CaAl_2O_4$ and $CaAl_4O_7$, i.e. slightly alumina rich monocalcium aluminates. The micrograph at 1400 °C prominently shows monoclinic crystallites that are different from the pseudohexagonal/orthorhombic structure at 930 °C [21]. With increase in temperature, monocalcium aluminate phases become prominent, reducing the amount of minor phases. Some authors suggest that at 1400 °C, calcium aluminate phase may show either monoclinic or orthorhombic polymorphic structure, depending on the kinetic limit of crystallization [26]. Chemical analysis also corroborates that CaO = 32.30% and Al_2O_3 = 67.70% (by weight), due to extra corundum phases at 1400 °C (Fig. 3b). It should also be made

clear that (AlO_6) groups and (Ca–O–Al) linkages mentioned before stood for spinel-type (AB_2O_4) compound in respect of the stoichiometric similarity [28]. AB_2O_4 crystal structure is of course cubic (unit cell) whereas $CaAl_2O_4$ reveals monoclinic or orthorhombic/pseudohexagonal structure depending on the thermal history. Ca-doped disordered γ-Al_2O_3 solid solution here is thus an intermediate product between 500 and 600 °C, which is poorly crystalline that gave rise to aggregated nanophases.

The Lewis acidic characteristics of doped γ-Al_2O_3 need to be emphasized in this context (Fig. 4a). It is well known that due to evolution of newly formed enormous surfaces, water can be adsorbed on the fine, lamellar, porous structure of defective spinel type cubic γ-Al_2O_3 phase derived from boehmite (γ-AlOOH) at 500 °C [29]. When calcined above 300 °C (Fig. 4a) it causes the loss of butanoic acid from boehmite surface and above 500 °C generates γ-Al_2O_3 [25]. As such the reactive γ-Al_2O_3 phase (derived from boehmitic species) contains finer nanopores that can readily adsorb water to result in a protospinel structure with one (OH) per unit cell [30]. We suggest that calcium ion enriched intermediate γ-Al_2O_3 phase retains similar feature and the hydroxyl groups around the unit cell aggregates behave as capping agents for the required nanophases of calcium aluminate [20]. During heat treatment of Ca-doped boehmite in between 500 and 600 °C, nascent metal oxides react progressively faster to accomplish the formation of disordered and poorly crystalline Ca-doped γ-Al_2O_3. In fact, the calcium ions doped/exchanged boehmite and respective γ-Al_2O_3 are indistinguishable from undoped boehmite and γ-Al_2O_3 by XRD pattern shown in Fig. 3b [25]. Further sintering and growth of these nanosized particles are inhibited by decomposition of nitrates, release of water vapour and other fugitives to mimic an auto-combustion process [19]. γ-AlOOH exists at certain pH as $[Al(H_2O)_6]^{3+}$ complex ion, where Al^{3+}

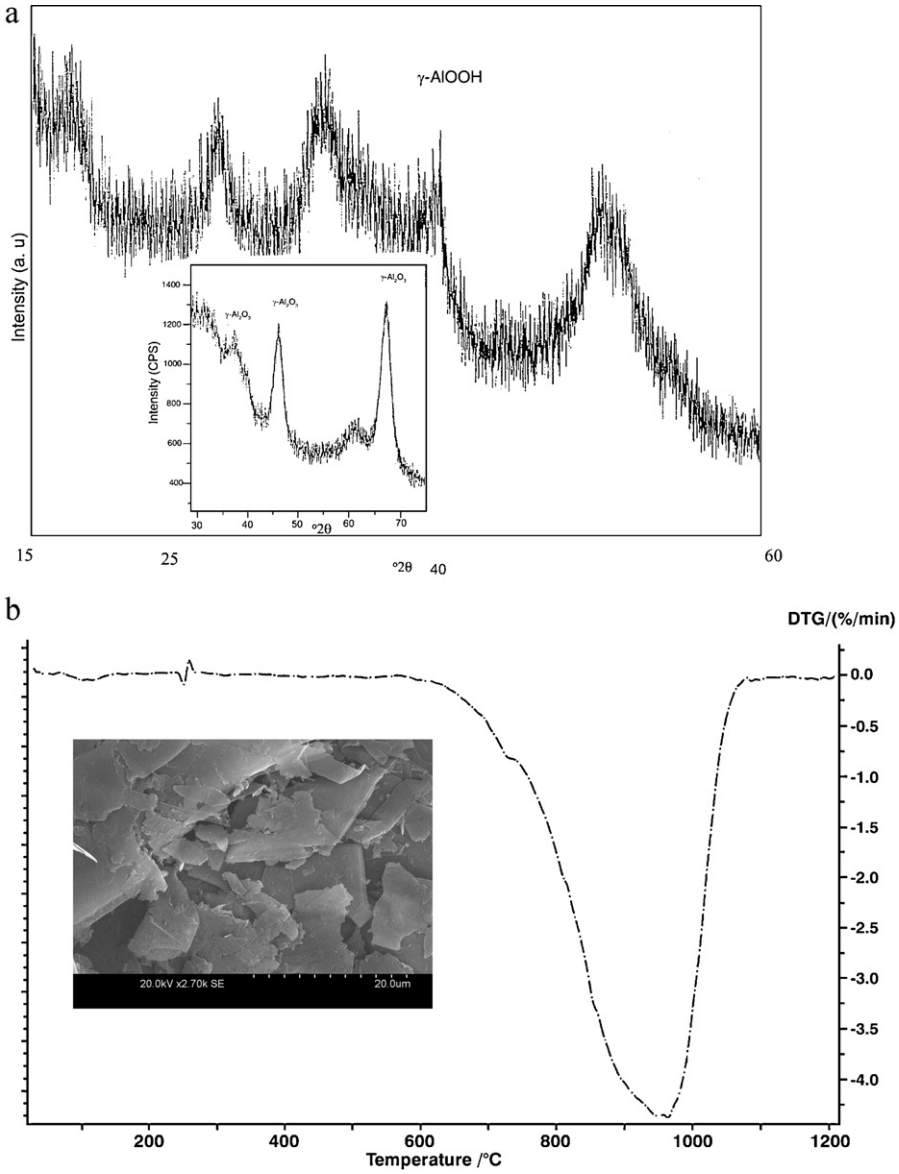

Fig. 4. (a) XRD patterns of boehmite gel precursor heat treated at 300 °C and 500 °C (inset) and (b) DTG pattern of as-received flaky graphite and its scanning electron micrograph (inset).

ions acting as Lewis acid pick up six pairs of electrons from neighbouring H_2O molecules (Lewis bases). This ion at 500 °C forms γ-Al_2O_3 with high surface area with many Al-sites exposed to result in active Lewis or Bronsted acid sites [31–33]. The surface acidity of γ-Al_2O_3 will definitely render it hydrophilic to readily adsorb polar molecules [29]. We strongly suggest that Ca-doped γ-Al_2O_3 will also retain this behavior, due additionally to water affinity of freshly generated nascent CaO regions in that solid solution. As clarified in our other papers [6,7], crystalline defects present in doped γ-Al_2O_3 should also interact efficiently with graphite underneath to develop a stable coating in between 500 and 600 °C. Thus when nanostructured thin films of Ca-doped γ-Al_2O_3 forms over graphite, the coated graphites acquire hydrophilicity with a lot of chemisorbed and physisorbed (OH) groups present over the modified surface. Fig. 4(b) shows the DTG plot of the uncoated graphite with its micrograph (inset). It is evident that starting from a conspicuous loss of graphite above 650 °C, another noticeable drop takes place around 900 °C. The depletion of graphite in refractory matrix would also start similarly with the onset of ceramic bonding in castable. It is thus necessary to arrest graphite oxidation quite earlier, near 650 °C, with a suitable sol gel coating that could form stable crystalline phases at that temperature (900 °C). In this respect, evolution of Ca-doped γ-Al_2O_3 in between 500 and 600 °C is important for $CaAl_2O_4$ phase evolution nearby 900 °C.

The AFM topography (Fig. 5a) of coated graphite shows nanosized calcium aluminate enriched particles sporadically

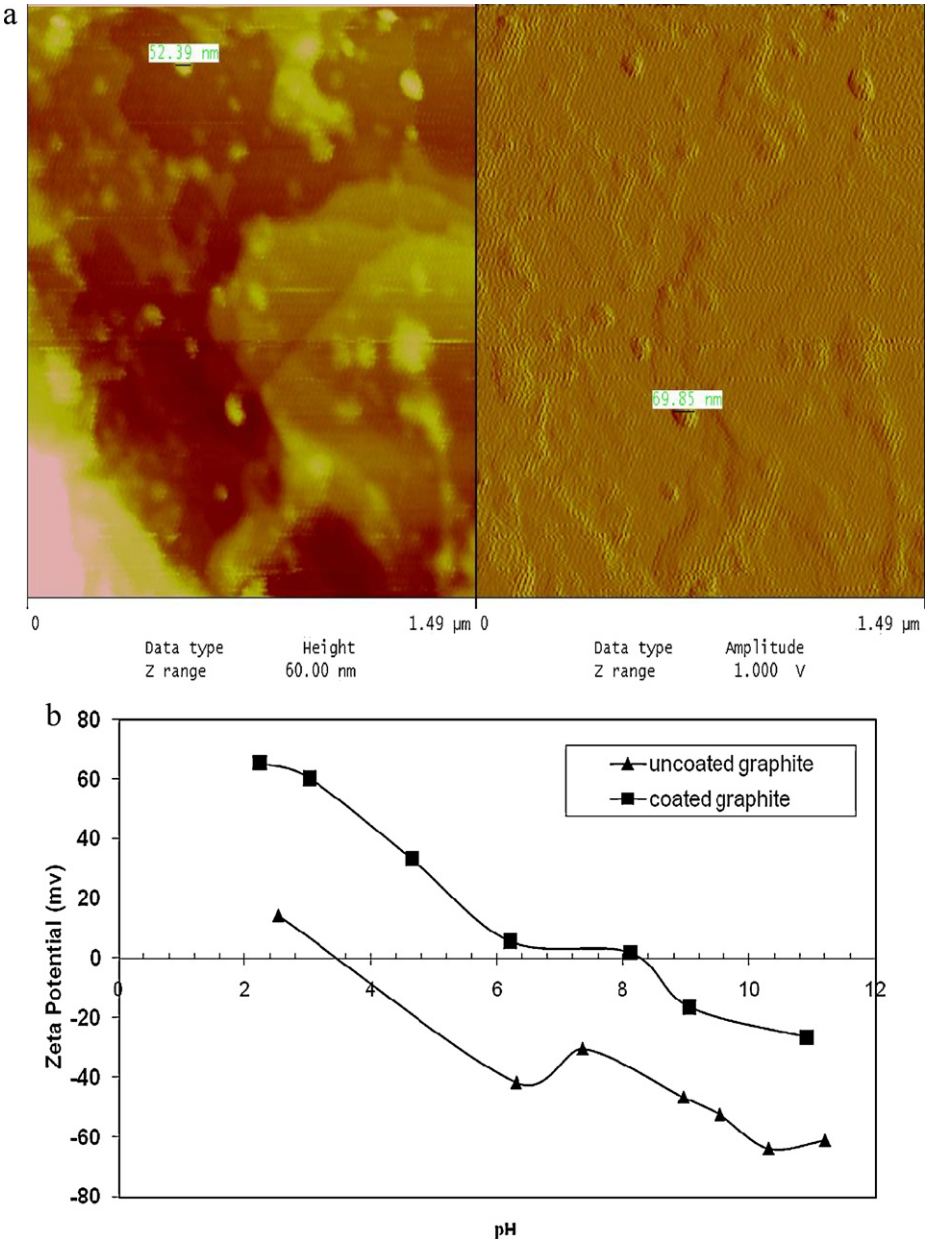

Fig. 5. (a) AFM surface topography of graphite coated by sol gel derived calcium aluminate and (b) Variation in zeta potential of coated and uncoated graphite with changing pH.

present at the surface. In addition, as the calcium aluminate precursor has been prepared at oxidizing condition in acidic pH, occasional formation of graphite oxide is also expected by hydrolysis and electrochemical oxidation [11,34]. As such enough of suitable sites can prevail superficially to exchange and hold the ionic species over the coating as well as to enhance its surface acidity [35]. It is well established that graphite oxide is also hydrophilic and it is hard to remove completely the intercalated water [36,37].

Fig. 5(b) shows a comparison between the pH vs zeta potential plots of as-received and coated graphites. The plot resolves that coated graphite would be more optimally suitable in the castable matrix with its two-fold beneficial effect. The dependence of viscosity on pH can be closely related to the zeta potential values of powders present in castable mix. At the isoelectric point, the almost neutral particle surfaces are brought closer due to the V.D. Waals attractive forces and coagulation causes viscosity enhancement. The high positive potential at low pH provides a high repulsive barrier between powder (oxide) particles to decrease the slurry viscosity. Similarly when pH increases beyond isoelectric point a repulsive potential is developed again to lower down the viscosity. However the viscosity rise intrinsically depends on particle size distribution of fine powders, their morphology, density, type and concentration of dispersing agents etc. [38]. Although various kinds of dispersants may work well, they are quite susceptible to failure when the quality of castable raw materials, e.g. impurities present, surface area etc. changes. In our case, the uncoated graphite is the main concern of the matrix and is associated with non-wettability in water from the very beginning. It demands higher amount of water to sufficiently lower down the viscosity of the mix. In contrast, using coated graphites, we can simultaneously control the optimum viscosity (or rheology) of the castable matrix and the improvement of hydrophilicity of coating to assure moisture reduction in castable. Although low viscosity is favourable for castable flow behavior, viscosity minima are not necessarily advantageous because it may lead to coarse and fine segregation [39]. Similarly very high viscosity values could make the flow of castable mix more restricted. In this regard the relationship between pH and zeta potential values of coated and uncoated graphites (Fig. 5b) is very important to obtain optimum matrix rheology. In this high alumina based matrix, spinel fines, microsilica, deflocculant, reactive alumina, etc., showed individual pH values below 8.0; however, when the matrix constituents were taken altogether in presence of high alumina cement, pH value of the slurry became closer to 8.5 and above (with or without graphite). In basic pH range a moderate increase of negative potential values of coated graphite will thus be preferred to the abrupt increase shown by the uncoated one, which may segregate the constituents. On the other hand, the higher positive potential of coated graphite at low pH values will enhance its dispersibility due to its association with hydrophilic functional groups (–COOH, –OH) which lower down the water demand during casting [5–7]. In contrast, as-received graphites contain either very low positive potential with very few ionic groups on the surface at low pH, or very high negative potential at higher pH values. Both of these adversely affect the matrix quality and deteriorate the flow property. It is thus expected that coated graphites with moderately lower zeta potential values (at pH $\geq$ 8.5) render good flowability with optimum viscosity [40]. Larger amount of nanosized hydrophilic species i.e. Ca-doped γ-Al_2O_3 phases in coated graphite, thus make it more easily dispersible to the aqueous medium [11]. We propose that it has been accomplished further by the presence of some intermittent surface oxidized graphite regions that strongly hold these ions. It is well documented that surface oxidized graphites may have both acidic (i.e. carboxylic –COOH, phenolic –OH) and basic (i.e. electron rich region in graphene layers) functional groups to impart surface charge in accordance with the pH of the solution [41,42]. Acidic functional groups e.g. (–COOH) and (–OH), are prominent in coated graphite at low pH regions [14], that are consistent with its hydrophilicity and acidic pH of coating formation. But hydrophobic functional groups are not so prominent in coated one (unlike as-received graphite) because (=C–H), (–C=C–) groups not arise sufficiently in the oxidizing condition and acidic pH of coating preparation.

Table 1
Changes in the physical properties of C^+ castable with temperature variation.

Properties	110 °C	900 °C	1500 °C
B.D. (g/cc)	2.83	2.70	2.88
A.P. (%)	24.6	29.5	21.0
CCS (kg/cm^2)	160	115	310

From the physical properties of (C^+) castable (Table 1), it is clear that its performance is quite comparable to those reported for the same castables prepared by spinel and mullite-coated graphites [5,6,8]. As the carbon content of graphite used in this study [14] is different from those previous reports, the BD, P and CCS values changed here a bit; however these are far better than the uncoated graphite containing castables (C^-). We already reported that (C^-) castable consumed 10.8% water unlike (C^+) type with 7.5% casting water; as such the green BD of (C^-) was significantly low (2.5 g/cm^3 from the very beginning. It is further clarified when the micrographs of fired (C^+) castables are examined in Fig. 6. The overall view of its microstructure (Fig. 6a) conforms to a dense contiguous structure with well sintered matrix. Plenty of hibonite crystallites are firmly interlocked with corundum and spinel grains due to the high temperature phase evolution in the refractory castable as explained elsewhere [43]. Some pores are sporadically present that could be reduced by avoiding aluminium powder addition in the batch. As the calcium aluminate coating itself improves the oxidation resistance of graphite, antioxidant aluminium powder is not essential for the (C^+) batch. This was added to maintain the compositional parity in both (C^+) and (C^-) batches; thus it can be advocated that further reduction in casting water in (C^+) castable would result in further improvement of properties compared with (C^-) castables [44]. Although calcium aluminate is prone to hydration, coated graphites do not pose such problem during storage and shipment; at the coating formation temperature

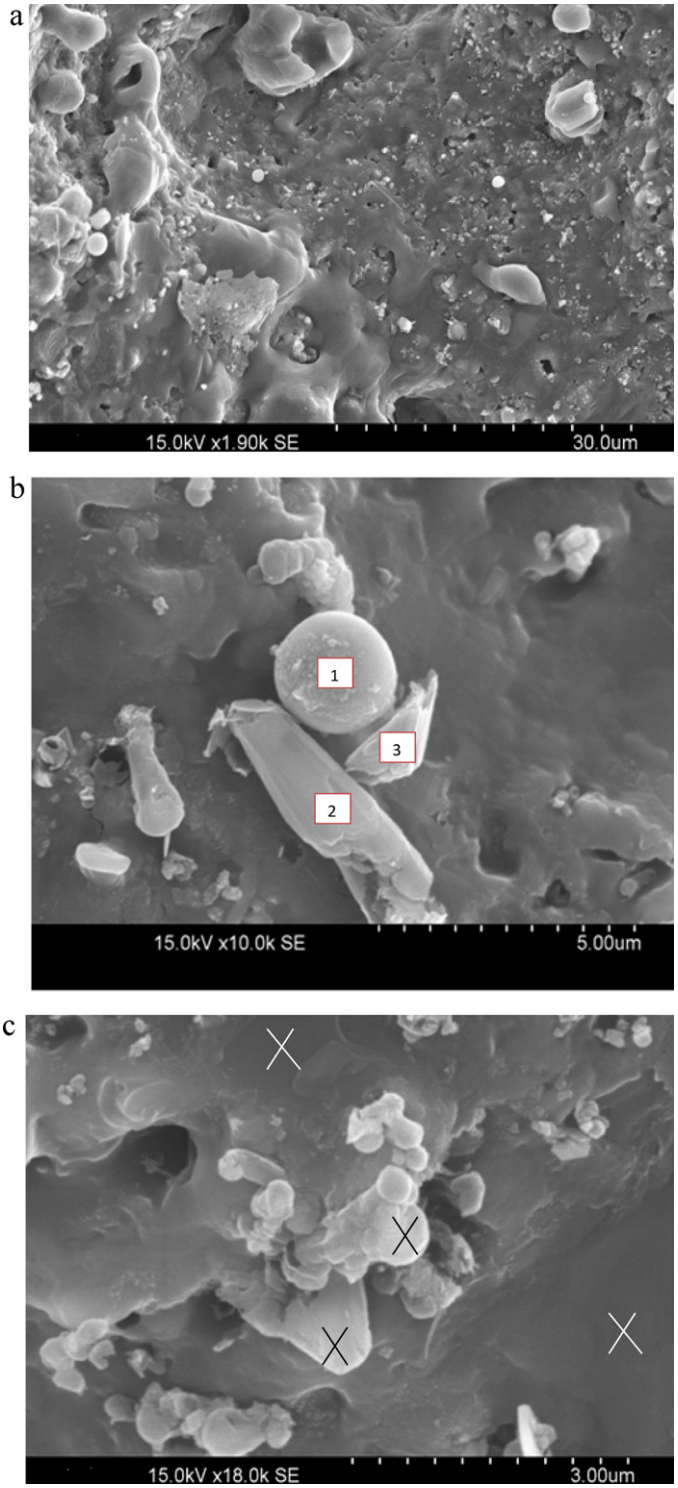

Fig. 6. (a) SEM micrograph (overall view) of C^+ castable fired at 1500 °C/5 h; (b) SEM (with EDS at three points) of C^+ castable fired at 1500 °C/5 h and (c) SEM of C^+ castable fired at 1500 °C/5 h.

(600 °C) only Ca-doped γ-Al_2O_3 is formed unlike well crystallized $CaAl_2O_4$ that develops beyond 900 °C. In addition, the thickness of coating being in micron scale, chances of extensive hydration is less prominent in comparison to that encountered in other cases, e.g. basic castables containing a huge amount of reactive MgO particles. More importantly proper ventilation, temperature and humidity of the storage condition should also be maintained to avoid hydration of this coated graphite.

Table 2
EDS results at three particular locations in Fig. 6b, the micrograph of C^+ castable (1500 °C).

Location	wt(%): C	O	Al	Si	Ca
Point 1	7.28	53.79	11.8	20.66	6.46
Point 2	54.18	23.33	7.97	9.73	4.79
Point 3	24.91	39.79	17.7	12.21	5.33

Table 2 shows the EDS data taken at three specific points (1, 2 and 3) in the micrograph shown in Fig. 6(b). Point 2 clearly shows that graphite is retained within the matrix of (C^+) castable after 5 h holding at exhaustive oxidizing atmosphere at 1500 °C. Points 1 and 3 suggest that graphites are surrounded by matrix enriched with C–A–S (C = CaO, A = Al_2O_3, S = SiO_2) phases. These viscous phases, together with the thin intermediate calcium aluminate coating, surely arrest graphite depletion. These retained graphites should improve the slag penetration and corrosion resistance of (C^+) castables. Very little graphites have been traced, however, in (C^-) castables after similar aggressive firing schedule. Unlike the (C^-) castables, the porosity of (C^+) has been decreased from the fabrication process due to its low water demand. Moreover, as the density of graphite is lower than the other oxide fines remaining in castable, loss of graphite in (C^-) castable accounts for additional porosity degradation. The EDS results corresponding to the other micrograph (Fig. 6c) infer furthermore the presence of carbon-enriched C–A–S and/or C–M–A–S regions (M = MgO). Cross-marked white regions showed compositions containing C (3–13%), O (42–53%), Al (18–21%), Si (16–20%), Ca (5–11%) and Mg (2.5–3.7%); whereas the cross-marked dark (grey) regions in Fig. 6(c) are consistent with C (7–21%), O (32–39%), Al (8–28%), Si (14–19%) and Ca (6–12%). Si and Mg are present obviously due to the microsilica and spinel ($MgAl_2O_4$) fines taken in the castable batch [43]. These indicate that sporadically present graphite rich regions are associated with C–A–S or C–M–A–S phases throughout the matrix. These not only help to reduce castable porosity, but also limit the debonding of graphites in the well sintered matrix and act as passivation layers to protect graphite from oxidation [45]. The thin calcium aluminate coating in the vicinity of graphite surface should also decrease the chances of decarburization during slag attack to the refractory [10]. Thus among the oxide-coated graphites reported so far, the calcium aluminate one may be considered a front-runner in future, simply due to its compatibility to both high alumina and basic castables. In our next publication, the concluding part of this work would focus on refractoriness and corrosion properties of such castables as reported in our previous paper [8].

4. Conclusion

This work is the continuation of our studies concerned with graphite coated by nanostructured calcium aluminates. From this laboratory scale investigation, it may be concluded that

unlike the commercial solid state method of production, the sol–gel synthesis yields calcium aluminate phases at much lower temperature. Nanosized Ca-doped γ-Al_2O_3, with strong Lewis acid sites, is an important intermediate for this chemical preparation. The comparison on pH and zeta potential values between uncoated and coated graphites establishes the suitability of the latter in castable mix. When such coating is developed on graphite surface at acidic pH and oxidizing atmosphere, its hydrophilicity is improved further. As a consequence the monolithic castable containing this surface-modified graphite consumes less water to show excellent physical properties and retains graphite in the matrix for a prolonged period. Together with the surrounding glassy phases, the thin calcium aluminate coating also acts as a passivation layer and enhances graphite bonding with the matrix part of high alumina castable.

Acknowledgements

The authors thankfully acknowledge Prof. T.K.Parya and Dr. P.K.Maiti of Dept. of Chemical Technology, and Dr. D.Chattopadhyay (Dept. of Polymer Sci. and Tech.), Calcutta University for their cooperation during the course of this investigation.

References

[1] M. Rigaud, S. Palco, N. Zhou, Alumina and magnesia-based castables containing graphite: comparison, in: 59th Electric Furnace Conference and 19th Process Technology Conference Proceedings 19, 2001, pp. 265–275.

[2] (a) S. Zhang, Next Generation Carbon Containing Refractory Composites, Advances in Sci. and Tech., vol. 45, Trans Tech Publications, Switzerland, 2006, pp. 2246–2253;
(b) S. Zhang, W.E. Lee, Improving the water-wettability and oxidation resistance of graphite using Al_2O_3/SiO_2 sol–gel coatings, J. Euro. Ceram. Soc. 23 (2003) 1215–1221.

[3] A.P. Luz, S. Ribeiro, V.G. Domiciano, M.A.M. Brito, V.C. Pandolfelli, Slag melting temperature and contact angle on high carbon containing refractory substrates, Ceramica 57 (2011) 140–149.

[4] A. Yamaguchi, Application of thermochemistry to refractories, in fundamentals of refractory technology, in: J.P. Bennett, J.D. Smith (Eds.), Ceramic Transactions vol. 125, The American Ceramic Society, OH 43081, USA, 2001, pp. 157–170.

[5] S. Mukhopadhyay, S. Dutta, Sk.A. Ansar, S. Das, S. Misra, Spinel-coated graphite for carbon containing refractory castables, J. Am. Ceram. Soc. 92 (8) (2009) 1895–1900.

[6] S. Mukhopadhyay, Improved sol gel spinel ($MgAl_2O_4$) coatings on graphite for application in carbon containing high alumina castables, J. Sol–Gel Sci. Technol. 56 (1) (2010) 66–74.

[7] Sk.A. Ansar, S. Bhattacharya, S. Dutta, S.S. Ghosh, S. Mukhopadhyay, Development of mullite and spinel coatings on graphite for improved water-wettability and oxidation resistance, Ceram. Int. 36 (2010) 1837–1844.

[8] S. Mukhopadhyay, et al., Characteristics of refractory castables containing mullite and spinel coated graphites, Mater. Manuf. Processes 27 (2) (2012) 177–184.

[9] EMM Ewais, Carbon based refractories (JAPAN), J. Ceram. Soc. Jpn. 112 (1310) (2004) 517–532.

[10] W.E. Lee, S. Zhang, Melt corrosion of oxide and oxide-carbon refractories, Int. Mater. Rev. 44 (3) (1999) 77–104.

[11] A. Saberi, F. Golestani-Fard, M. Willert-Porada, R. Simon, T. Gerdes, H. Sarpoolaky, Improving the quality of nanocrystalline $MgAl_2O_4$ spinel coating on graphite by a prior oxidation treatment on the graphite surface, J. Euro. Ceram. Soc. 28 (2008) 2011–2017.

[12] V. Roungos, C.G. Aneziris, H. Berek, E. Skiera, C. Thomser, Advances of nanoscaled additives on the thermo-mechanical performances of Al_2O_3–C and MgO–C refractories, Refractories Worldforum 4 (1) (2012) 91–104.

[13] (a) K. Kawabata, H. Yoshimatsu, E. Fuji, K. Hiragushi, A. Osaka, Properties of Al_2O_3–C castable refractories with graphite powder coated with alumina, J. Ceram. Soc. Jpn. 109 (2001) 270–273;
(b) X. Liu, S. Zhang, Low temperature preparation of titanium carbide coatings on graphite flakes from molten salts, J. Am. Ceram. Soc. 91 (2008) 667–670.

[14] S. Mukhopadhyay, G. Das, I. Biswas, Nanostructured cementitious Sol–gel coating on graphite for application in monolithic refractory composites, Ceram. Int. 38 (2) (2012) 1717–1724.

[15] (a) A.A. Goktas, M.C. Weinberg, Preparation and crystallization of sol–gel calcia–alumina compositions, J. Am. Ceram. Soc. 74 (5) (1991) 1066–1070;
(b) M. Uberoi, S.S. Risbud, Processing of amorphous calcium aluminate powders at <900 °C, J. Am. Ceram. Soc. 73 (6) (1990) 1768–1770.

[16] R.K. Pati, A.B. Panda, P. Pramanik, Preparation of nanocrystalline calcium aluminate powder, J. Mater. Synth. Process. 10 (4) (2002) 157–161.

[17] D. Stephan, P. Wilhelm, Synthesis of pure cementitious phases by sol–gel process as precursor, Z. Anorg. Allg. Chem. 630 (2004), 1477–1425.

[18] M.F. Zawrah, N.M. Khalil, Synthesis and characterization of calcium aluminate nanoceramics for new applications, Ceram. Int. 33 (8) (2007) 1419–1425.

[19] (a) S. Kurajica, G. Mali, T. Gazivoda, J. Sipusic, V. Mandic, A spectroscopic study of calcium aluminate gels obtained from aluminium sec-butoxide chelated with ethyl acetoacetate in various ratios, J. Sol–Gel Sci. Technol. 50 (2009) 58–68;
(b) S. Kurajica, V. Mandic, J. Sipusic, Thermal evolution of calcium aluminate gel obtained from aluminium-sec-butoxide chelated with ethylacetoacetate, J. Ceram. Sci. Tech. (2010), doi:10.4416/JCST 2010-00017.

[20] A. Banerjee, S. Das, S. Misra, S. Mukhopadhyay, Structural analysis of spinel ($MgAl_2O_4$) for application in spinel-bonded castables, Ceram. Int. 35 (2009) 381–390.

[21] K.L. Scrivener, A. Campas, Calcium Aluminate Cements, in: P.C. Hewlett (Ed.), Lea's Chemistry of Cement and Concrete, 4th ed., Butterworth-Heinemann, Oxford, 2001 , pp. 709–778 (Chapter 13).

[22] N.B. Singh, N.P. Singh, Formation of CaO from thermal decomposition of calcium carbonates in presence of carboxylic acids, J. Therm. Anal. Calorim. 89 (1) (2007) 159–162.

[23] S. Iftekhar, et al., Phase formation of $CaAl_2O_4$ from $CaCO_3$–Al_2O_3 powder mixtures, J. Euro. Ceram. Soc. 28 (2008) 747–756.

[24] (a) B.M. Mohamed, J.H. Sharp, Kinetics and mechanism of formation of monocalcium aluminate, $CaAl_2O_4$, J. Mater. Chem. 7 (8) (1997) 1595–1599;
(b) E. Chabas, D. Goeuriot, Effects of alumina powder characteristics on the reactive sintering of CaO–Al_2O_3, Mater. Ceram./Ceram. Mater. 62 (3) (2010) 239–243.

[25] (a) A. Kareiva, C. Jeff Harlan, D. Brent MacQueen, R.L. Cook, A.R. Barron, Carboxylate-substituted alumoxanes as processable precursors to transition metal−aluminum and lanthanide–aluminum mixed-metal oxides: atomic scale mixing via a new transmetalation reaction, Chem. Mater. 8 (1996) 2331–2340;
(b) R. Cook, M. Kochis, I. Reimanis, H.-J. Kleebe, A new powder production route for transparent spinel windows: powder synthesis and window properties, in: R.W. Tustison (Ed.), SPIE Defence and Security Symposium Proceedings Vol. 5786 IX. Window and Dome Technologies and Materials (Orlando/FL, 28. 3. 2005), The Society of Photo-Optical Instrumentation Engineers, Bellingham, WA, 2005, pp. 41–47.

[26] A. Douy, M. Gervais, Crystallisation of amorphous precursors in the calcia – alumina system: a differential scanning calorimetry study, J. Am. Ceram. Soc. 83 (1) (2000) 70–76.

[27] A.E. Lavat, M.C. Grasselli, E.G. Lovecchio, Effect of α and γ-polymorphs of alumina on the preparation of $MgAl_2O_4$ – spinel – containing refractory cements, Ceram. Int. 36 (1) (2010) 15–21.

[28] J.J. Vijaya, L.J. Kennedy, G. Sekaran, K.S. Nagaraja, Utilisation of Sr(II) added calcium aluminate for the detection of volatile organic compounds, Ind. Eng. Chem. Res. 46 (19) (2007) 6251–6258.
[29] Y. Arai, Chemistry of Powder Production, Chapman and Hall, New York, 1996, pp. 49–70.
[30] G. Paglia, et al., Boehmite-derived γ-alumina system.2: consideration of hydrogen and surface effects, Chem. Mater. 16 (10) (2004) 1914–1923.
[31] D. Guillaume, S. Gautier, I. Despujol, F. Alario, P. Beccat, Characterization of acid sites on γ-Al_2O_3 and chlorinated γ-Al_2O_3 by ^{31}P NMR of adsorbed trimethylphosphine, Catal. Lett. 43 (3-4) (1997) 213–218.
[32] L. Pejov, T. Skapin, Adsorption of pyridine on the lewis acid sites of microcrystalline γ-alumina: a quantum chemical cluster model study, Chem. Phys. Lett. 400 (2004) 453–461.
[33] X. Liu, R.E. Truitt, DRFT-IR studies on surface of γ-Al_2O_3, J. Am. Chem. Soc. 119 (41) (1997) 9856–9860.
[34] N.E. Sorokina, et al., Anodic oxidation of graphite in 10–98% HNO_3, Inorg. Maters. 37 (2001) 360–365.
[35] (a) C. Moreno-Castilla, et al., Effects of non-oxidant and oxidant acid treatments on the surface properties of an activated carbon with very low ash content, Carbon 36 (1998) 145–151;
(b) C. Moreno-Castilla, et al., Changes in surface chemistry of activated carbons by wet oxidation, Carbon 38 (2000) 1995–2001.
[36] S. Cerveny, et al., Dynamics of water intercalated in graphite oxide, J. Phy. Chem. C 114 (2010) 2604–2612.
[37] A. Lerf, et al., Hydration behavior and dynamics of water molecules in graphite oxide, J. Phy. Chem. Solids 67 (2006) 1106–1110.
[38] A.R. Studart, V.C. Pandolfelli, J. Gallow, Dispersants for high alumina Castables, Am. Ceram. Soc. Bull. 81 (2002) 36–44.
[39] P. Bonadia, A.R. Studart, R.G. Pileggi, V.C. Pandolfelli, S.L. Vendrasco, Applying MPT principle to high alumina castables, Am. Ceram. Soc. Bull. 78 (3) (1999) 57–60.
[40] S. Otroj, et al., The effect of deflocculants on the self-flow characteristics on ultra-low cement castables in Al_2O_3–SiC–C system, Ceram. Int. 31 (2005) 647–653.
[41] M. Alazemi, et al., Electrically conductive thin films prepared from layer-by-layer assembly of graphite platelets, Adv. Funct. Mater. 19 (2009) 1118–1129.
[42] C. Moreno–Castilla, Adsorption of organic molecules from aqueous solution on carbon materials, Carbon 42 (2004) 83–94.
[43] S. Mukhopadhyay, T.K. Pal, P.K. DasPoddar, Improvement of corrosion resistance of spinel-bonded castables to converter slag, Ceram. Int. 35 (2009) 373–380.
[44] S. Banerjee, Monolithic Refractories: A Comprehensive Handbook, The American Ceramic Society, Westerville, OH, USA, 1998, pp. 56–61.
[45] M. Rigaud, Corrosion of industrial refractories, in: J.P. Bennett, J.D. Smith (Eds.), Fundamentals of Refractory Technology, Ceramic Transactions, vol. 125, The American Ceramic Society, OH 43081, USA, 2001, pp. 135–154.